15TH IEA HEAT PUMP CONFERENCE
MAY 26–29, 2026 | HOFBURG
VIENNA 2026
DECARBONISATION THROUGH INNOVATION

Techno-economic assessment of the advantages of small-scale turbo compressor adoption within brine-to-water heat pump

Alessandro Panzeri[a,*], Konstantinos Kontomaris[b], Jürg Alexander Schiffmann[a]

[a]Laboratory for Applied Mechanical Design, Ecole Polytechnique Fédérale de Lausanne, Rue de la Maladière 71b, CH-Neuchâtel 2000, Switzerland

[b]Chemours, Fluorochemicals R&D, Wilmington, DE, USA

Abstract

This paper presents and discusses the results of a research study focused on the technological advancement of heat pump systems, with the primary objective of reducing their Total Cost of Ownership (TCO) and assessing the feasibility of low-pressure refrigerants as low-environmental-impact alternatives to currently marketed fluids. The study investigates the replacement of traditional scroll compressors with small-scale turbo compressors in brine-to-water vapor compression heat pump cycles operating at three power levels — 5 kW, 15 kW, and 100 kW — representative of small domestic, light commercial, and large commercial applications. The analysis is based on numerical simulations of two single-stage heat pump configurations: one equipped with a scroll compressor and the other with a turbo compressor. The simulations are performed using a custom numerical environment and a standard thermophysical property database, and incorporate a range of medium- and low-pressure refrigerants: R32, R290, R1234yf, R152a, R134, R1234ze(E), R1336mzz(E), R1234ze(Z), R1233zd(E), and R1336mzz(Z). The turbo compressor is modelled using an experimentally validated in-house 0D model, while the scroll compressor isentropic efficiency is estimated based on manufacturer performance selection software. The performance of both systems is evaluated under operating conditions defined by the European Standard EN 14825. The TCO is annualized and includes purchase cost, installation cost, and energy consumption over a 20-year lifetime, with a 5% interest rate applied to account for cost discounting. Results suggest that the adoption of a turbo compressor enables significant TCO reduction, mainly due to higher Seasonal Coefficient of Performance (SCOP) and smaller, more efficient heat exchangers. This improvement is driven by the turbo compressor's ability to modulate power output and maintain high isentropic efficiency across different operating conditions. In addition, the use of gas bearings eliminate the need for oil lubrication, which prevents refrigerant contamination and enhances heat exchanger performance.

Selection and/or peer-review under the responsibility of the organizers of the 15th IEA Heat Pump Conference 2026.

Keywords: Heat pump; Turbo compressor; Scroll compressor; Total Cost of Ownership; SCOP

1. Introduction

The continuous rise in global average temperatures, as reported by the Intergovernmental Panel on Climate Change (IPCC) in its Sixth Assessment Report [1-2], highlights the urgency of reducing greenhouse gas emissions and accelerating the transition toward sustainable and low-carbon energy systems. According to the International Energy Agency (IEA) [3], the residential heating and cooling sector accounts for a substantial share of global energy use and CO_2 emissions — nearly 30% and over one-quarter respectively — making it a key focus for decarbonization efforts.

Among available technologies, high-efficiency heat pumps have emerged as one of the most promising solutions to meet both environmental and energy policy targets. According to the International Energy Agency (IEA) [4], accelerating their deployment is essential to achieving net-zero goals, as heat pumps can deliver large reductions in primary energy demand and CO_2 emissions compared to fossil-based systems [5]. The phase-out of hydrofluorocarbon (HFC) refrigerants under the Kigali Amendment and the new EU Regulation

* Corresponding author. Tel.: +41-21-693-45-23
E-mail address: alessandro.panzeri@epfl.ch

2024/573 further emphasizes the need for technological innovation in both system components and working fluids. In this context, small-scale turbo-compressors offer high isentropic efficiency and compactness compared to conventional positive-displacement machines [6].

This study investigates the impact of integrating a small-scale turbo-compressor into a domestic heat pump cycle in terms of TCO at three representative power levels — 5, 15, and 100 kW — simulating the use of mid- and low-pressure fluids. For each fluid, the TCO was calculated and optimized at 5, 15, and 100 kW using both scroll and turbo compressor technologies. To evaluate the results from a market perspective, the optimum TCO values obtained with turbo compressors were compared to the scroll-based TCO of R32, which serves as the benchmark in this analysis. Additionally, for each fluid, the turbo-based TCO was also compared to the scroll-based TCO using the same fluid. This dual comparison allows for both a scientific assessment of performance and an evaluation of commercial feasibility.

2. Methods

2.1. Heat pump model

2.1.1. Cycle design

The considered plant is a brine-to-water, single-stage vapor compression heat pump representative of a ground-source floor heating system. It is simulated with the mid- and low-pressure refrigerants listed in Table 1. Thermodynamic properties of all fluids were calculated using REFPROP v10 [7]. Water and brine are used as secondary fluids on the condenser and evaporator sides; the brine, following Melinder [8], is a water–propylene glycol mixture (0.671/0.329 mass fraction) ensuring freeze protection down to –15 °C. A fixed 5 °C temperature difference is imposed across both circuits.

The unit is designed to meet the annual heating demand for a moderate climate zone defined by EN 14825 [9] and shown in Table 2. Two configurations are analyzed: one using a turbo compressor and the other a scroll unit. In the turbo layout, compressor and heat exchangers are dimensioned and optimized for the Design point (100% load). In the scroll layout, compressor data are derived from manufacturer-provided selection tools, with heat exchangers sized for full-load operation. A fouling factor is included to account for oil circulation in the scroll system, whereas it is omitted in the oil-free turbo case. Off-design performance is evaluated for both.

Table 1. Refrigerant properties: family, formula, molar mass and normal boiling point (NBP).

Refrigerant	Family	Formula	Molar Mass [kg/kmol]	NBP [°C]
R32	HFC	CH2F2	52.02	-51.65
R290	HC	CH3CH2CH3	44.10	-42.11
R1234yf	HFO	CF3CF=CH2	114.04	-29.48
R152a	HFC	CHF2CH3	66.05	-24.02
R134	HFC	CHF2CHF2	102.53	-19.28
R1234ze(E)	HFO	CHF=CHCF3	114.04	-18.97
R1336mzz(E)	HFO	CF3CH=CHCF3 (trans)	164.05	7.86
R1234ze(Z)	HFO	CHF=CHCF3 (cis)	114.04	9.72
R1233zd(E)	HFO	CF3CH=CHCl	130.50	18.26
R1336mzz(Z)	HFO	CF3CF=CHCF3 (cis)	164.06	33.45

Table 2. Operating points used for the simulation of the heat pump according to EN 14825.

Point	Load %	Powers [kW]			T water [°C]	T brine [°C]	Hours [h]
		Power 1	Power 2	Power 3			
Design	100	5.00	15.00	100.00	35.0	0.0	0
A	88	4.40	13.20	88.00	34.0	0.0	348
B	54	2.70	8.10	54.00	30.0	0.0	1893
C	35	1.75	5.25	35.00	27.0	0.0	1645
D	15	0.75	2.25	15.00	24.0	0.0	1024

To minimize the TCO, the system was assessed for the nine pinch temperature combinations reported in Table 3. Condensing and evaporating temperatures were defined by the imposed pinch values on each side of the cycle. Subcooling and superheating were initially set to 0.1 °C to ensure heat transfer occurred mainly during phase change, with superheating adjusted later for each refrigerant to keep the compressor discharge in the superheated vapor region.

Table 3. Main pinch combinations assumed in the analysis.

Evaporator		2 [°C]	5 [°C]	8 [°C]
Condenser	2 [°C]	(2, 2)	(2, 5)	(2, 8)
	5 [°C]	(5, 2)	(5, 5)	(5, 8)
	8 [°C]	(8, 2)	(8, 5)	(8, 8)

2.1.2. Turbo compressor model

Turbo compressor units were individually designed to maximize isentropic efficiency for each refrigerant at the Design operating point and for all pinch combinations. The design followed the approach of Schiffmann et al. [10], determining key parameters such as rotational speed, impeller and magnet dimensions, bearing diameters and clearances, and overall rotor weight (Figure 1, Table 4). Fixed design parameters include specific speed $n_s = 0.44$, bearing number $ND_m = 2.6 \times 10^6$ rpm mm, motor shear stress $\tau = 18$ kPa, and motor tip speed $v_{tip} = 180$ m/s. The model automatically selects the gas-lubricated bearing type based on load capacity, considering Herringbone Grooved Journal Bearings (HGJB) and Gas Foil Bearings (GFB). HGJBs offer higher efficiency but lower load capacity; when both are feasible, the more efficient HGJB is preferred. The rotor-bearing system is verified for load capacity and dynamic stability, and an Eigenfrequency analysis ensures the first critical bending frequency exceeds 1.25 × the maximum operating speed, thus avoiding excitation of the first bending mode. Once geometry is defined, compressor performance is evaluated under off-design conditions across the full operating range.

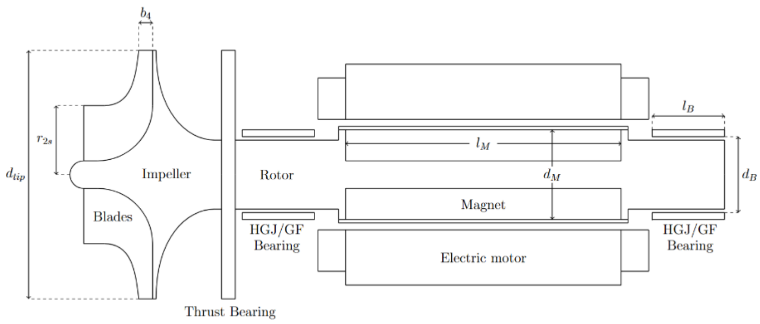

Figure 1. Scheme of the compressor and indication of its design parameters.

Table 4. Turbo compressor main design parameters.

Description	Symbol
Impeller tip diameter	d_{tip}
Inlet shroud radius	r_{2s}
Tip blade height	b_4
Journal bearing diameter	d_B
Journal bearing length	$l_B = d_B$
Journal bearing clearance	c_0
Magnet diameter	d_M
Magnet length	l_M
Rotational speed	n_{rot}
Rotor mass	m_r

2.1.3. Scroll compressor model

Scroll compressor sizing and performance were obtained using manufacturer selection software, which identifies suitable compressor units based on refrigerant type, operating conditions, and required heat load. Compatible scroll models were directly available for R290 at 5 kW and 15 kW. For the remaining fluids — R32, R1234yf, R152a, R134, R1234ze(E), R1336mzz(E), R1234ze(Z), R1233zd(E), and R1336mzz(Z) — no direct matches were found. In these cases, R134a, R290, and R454B were adopted as surrogate fluids for compressor selection purposes, owing to their similar pressure and volumetric characteristics under comparable conditions: R134a for R152a, R134, and R1234ze(E); R290 for R32 at 5 kW and 15 kW; and R454B for R32 and R1234yf at 100 kW. No scroll compressors were identified for the remaining fluids due to the much higher pressure and volume ratios. Overall, the pressure ratio (PR) and volumetric ratio (VR) deviations between operating and surrogate fluids remained within ±8%, specifically: for R134a-based selections, R152a (+1.15% PR, +0.96% VR), R134 (–6.30%, –5.22%), and R1234ze(E) (–2.57%, –2.14%);

for R290-based selections, R32 (–7.20%, –5.96%); and for R454B-based selections, R32 (+0.07%, +0.06%) and R1234yf (–7.83%, +6.49%).

A MATLAB function was finally developed to reproduce scroll compressor performance within the simulation environment. For each model, the function interpolates manufacturer data of isentropic efficiency and mass flow rate over the full operating envelope.

2.1.4. Plate heat exchangers

Given the working fluids — water in the condenser and brine in the evaporator — plate heat exchangers (HEXs) were selected as the most suitable configuration. As for the turbo compressor, both condenser and evaporator were designed and optimized for each pinch-point condition to deliver the thermal load at design power. The adopted model, developed by Amalfi [11], simplifies the HEX to a single refrigerant–plate–water interface, where the mass flow per fluid and interface equals the total flow divided by (Np/2 + 1), Np being the total number of plates. Using plate geometry and inlet conditions of both fluids, it computes overall heat-transfer coefficient and pressure drop in 1 mm increments along the plate length. The main geometrical parameters: plate length L_p, width w, thickness t, Chevron angle β, peak-to-valley distance b, corrugation wavelength λ, and port diameter d_p are predefined (Figure 2). The corrugation aspect ratio γ (1) quantifies corrugation intensity, while the enlargement factor ϕ (2) represents the additional surface area generated.

$$\gamma = \ 2b/\lambda \tag{1}$$

$$\phi \approx 1/6\ (1 + \sqrt{(1 + (b\pi/\lambda)^2)} + 4\sqrt{(1 + 1/2 \cdot (b\pi/\lambda)^2)}) \tag{2}$$

The plate width, maximum number of plates, and length-to-width ratio were defined according to the maximum refrigerant volumetric flow rate $\dot{V}$, based on typical commercial heat exchanger catalogues. Adopted values, listed in Table 5, reflect standard commercial plate heat exchanger designs. The number of plates and plate length were treated as design variables in the optimization process. The design ranges based on commercial products are reported in Table 6. For the scroll-based system, the presence of oil diluted in the refrigerant was accounted for through a fouling factor of $1.67 \cdot 10^{-4}$ m²·K/W, as suggested by Sinnott and Towler [12]. No fouling was considered for the oil-free turbo-based heat pump heat exchangers.

Table 5. Main design parameters of the plate heat exchanger.

Parameter	Symbol	Value
Number of plates	N_p	Optimization variable
Plate length	L_p	Optimization variable
Plate width	w	$f(\dot{V})$ [mm]
Length/width ratio	$r_{l/w}$	$f(\dot{V})$
Plate thickness	t	0.5 [mm]
Chevron angle	β	60 [°]
Peak-to-valley distance	b	1.2 [mm]
Corrugation wavelength	λ	6 [mm]
Port diameter	d_p	0.25 · w [mm]
Enlargement factor	ϕ	1.09
Corrugation aspect ratio	γ	0.4

Table 6. Design parameter ranges as a function of volumetric flow rate $f(\dot{V})$, based on typical commercial heat exchanger specifications.

$\dot{V}$ [m³/h]	N_p [-]	w [mm]	$r_{l/w}$ [-]
$0 < \dot{V} \leq 5$	$10 \leq N_p \leq 70$	75	$0.5 \leq r_{l/w} \leq 8$
$5 < \dot{V} \leq 20$	$10 \leq N_p \leq 150$	120	$0.5 \leq r_{l/w} \leq 6$
$20 < \dot{V} \leq 100$	$10 \leq N_p \leq 250$	200	$0.5 \leq r_{l/w} \leq 4$
$\dot{V} > 100$	$10 \leq N_p \leq 350$	300	$0.5 \leq r_{l/w} \leq 3$

The heat exchangers were sized to meet design loads of 5 kW, 15 kW, and 100 kW for the condensers, and corresponding evaporator loads derived from the cycle model, for each refrigerant, compressor type, and pinch-point configuration at Design point. The optimization was performed separately for the condenser and evaporator using the BORG multi-objective evolutionary algorithm [13]. In both cases, the objectives were to minimize heat transfer area (3.1) and pressure drop (3.2) under several constraints (3.3–3.5). Due to the discrete nature of design increments, a heat transfer tolerance Q_{Toll} was applied. The maximum allowable pressure drop was expressed as a temperature drop $\Delta T_{HEX,lim}$ along the condensation or evaporation process. A minimum mass flux threshold $G_{HEX,lim}$ was imposed to ensure sufficient flow inertia and avoid stagnation or recirculation at low velocities. For R32, R290, R1234yf, R152a, R134, and R1234ze(E), optimizations applied a heat transfer tolerance of ±0.5%, temperature drop limits due to pressure drop of $\Delta T_{Cond,lim}$ = 0.4 °C and $\Delta T_{Evap,lim}$ = 0.8 °C, and a minimum mass flux $G_{HEX,lim}$ = 8 kg/(m^{2}s). For the higher-boiling fluids R1336mzz(E), R1234ze(Z), R1233zd(E), and R1336mzz(Z), the same values were used except for $\Delta T_{Evap,lim}$ = 1.8 °C. Finally, given the conflicting nature of the two objectives — smaller heat transfer areas typically increasing pressure drops — a Pareto front was generated for each refrigerant and pinch configuration, identifying the optimal trade-offs (Figure 3).

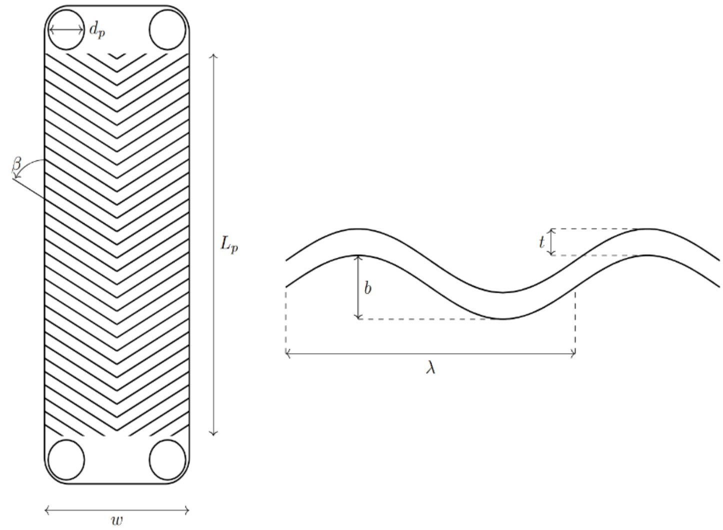

Figure 2. Main design parameters of the plate.

$$min_{N_{p,HEX},L_{p,HEX}} A_{HEX}\left(N_{p,HEX}, L_{p,HEX}\right) \tag{3.1}$$

$$min_{N_{p,HEX},L_{p,HEX}} \Delta P_{HEX}\left(N_{p,HEX}, L_{p,HEX}\right) \tag{3.2}$$

$$\left|1 - \frac{Q_{HEX,calc}}{Q_{HEX}}\right| < Q_{Toll} \tag{3.3}$$

$$1 - \frac{\Delta T_{HEX,calc}}{\Delta T_{HEX,lim}} > 0 \tag{3.4}$$

$$1 - \frac{G_{HEX,plate}}{G_{HEX,lim}} < 0 \tag{3.5}$$

Among the Pareto-optimal solutions, the final design prioritized minimizing heat transfer area while allowing pressure drops up to 10 kPa. Further analyses suggested that below this limit, area reduction affects the TCO far more than pressure losses, yielding configurations that balance compactness and efficiency.

2.2. Economic model

2.2.1. Total cost of ownership

TCO is calculated as the sum of the Capital Expenditure (CAPEX) over a 20-year investment horizon, assuming an interest rate of 5%, and Operating Expenditure (OPEX).

$$TCO = CAPEX + OPEX \tag{4}$$

For each refrigerant and compressor configuration, TCO was calculated for all pinch combinations listed in Table 3. The global minimum for the optimal pinch combination was determined via spline interpolation.

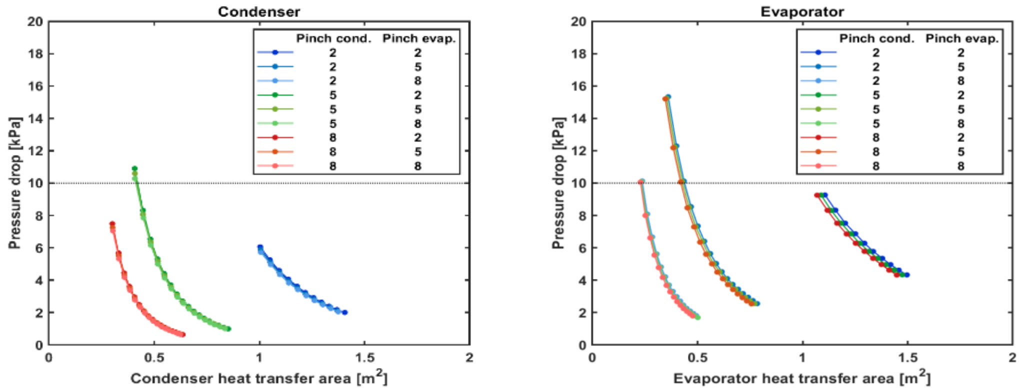

Figure 3. Example of Pareto fronts for both the condenser (a) and the evaporator (b) designs.

2.2.2. Capital expenditure

CAPEX represents the annualized total investment cost of the system, obtained from the sum of the main component costs — compressor (scroll or turbo), condenser, evaporator, and working fluid. To include auxiliary equipment (piping, valves, controls), transportation, and installation, this base cost is multiplied by a factor $k = 6.32$, as recommended by Auracher [14] for new systems. The total investment is then annualized using the Capital Recovery Factor (CRF), which converts it into an equivalent yearly expense over the system lifetime:

$$CRF = \frac{i\cdot(1+i)^n}{(1+i)^n - 1} \tag{5}$$

where i = 5% is the annual interest rate and n = 20 years the investment horizon. An additional factor f = 1.05 accounts for the extra cost associated with highly flammable fluids such as R290, according to Wei et al. [15]. The resulting annualized cost is thus:

$$CAPEX = (Compressor\ cost + Condenser\ cost + Evaporator\ cost + Fluid\ cost)\cdot k \cdot CRF \cdot f \tag{6}$$

The baseline cost of the turbo compressor was assumed to be 500 CHF for a 2 kW unit, under the condition of mass production exceeding 1,000 units per year, as indicated by Mounier [16]. This reference cost is consistent with our analysis for the 5 kW system, which employs compressors with shaft power in the range of 1–1.5 kW. For the same system, an identical base cost was initially considered for the scroll compressor. According to Olympios et al. [17], the cost of scroll compressors scales almost linearly with volumetric flow rate, and consequently with power output. Therefore, the cost of scroll compressors was scaled linearly starting from the 500 CHF reference value to match the power levels of the other systems. Given that scroll and turbo compressors have comparable cost magnitudes, the same scaling approach was applied to turbo compressors. The resulting estimated costs for both compressor types were finally assumed to be 500 CHF, 1,500 CHF, and 10,000 CHF, for the 5 kW, 15 kW, and 100 kW heat pumps, respectively.

The cost of heat exchangers primarily depends on their heat transfer area. Based on Henchoz et al. [18], the cost of plate heat exchangers can be estimated from the condenser and evaporator heat transfer areas as follows:

$$Heat\ exchanger\ cost = 147 + 407 \cdot A_{HEX} \tag{7}$$

The refrigerant cost was calculated as the product of the system refrigerant charge (kg) and a unit price of 50 CHF/kg, based on indicative pricing provided by the refrigerant manufacturer. For consistency, this cost was assumed constant across all fluids:

$$Fluid\ cost\ =\ 50 \cdot m_{ref} \tag{8}$$

2.2.3. Operating expenditure

OPEX represents the annual energy cost of heat pump operation, and is evaluated by integrating the energy consumption over all the operating bins i defined by EN 14825:

$$OPEX\ =\ \sum_i \frac{Q_{Cond,i}}{COP_i} \cdot h_i \cdot e \tag{9}$$

where i denotes the operating condition; $Q_{Cond,i}$ is the condenser heat output [kW]; COP_i [-] the coefficient of performance; h_i the operating hours [h/yr]; and e = 0.3 [CHF/kWh] the 2024 Swiss average electricity cost. Changes in operating conditions modify heat-exchanger temperatures and refrigerant mass flow to meet the required load. The scroll compressor operates at fixed speed, resulting in on–off cycling as load decreases. In the turbo compressor system, rotor speed is adjusted either to match the required mass flow or to reach the minimum flow before surge, which may also induce on–off operation. Because a lower temperature lift — thus lower pressure ratio — reduces the required speed and mass flow, turbo compressors naturally adapt to variable thermal loads. Part-load and cycling effects are corrected per EN 14825 using a degradation factor $C_d = 0.9$ and the capacity ratio CR accounting for the ratio user heat demand over delivered heat:

$$COP_i = COP_{Cycle,i} \cdot \frac{CR}{C_d \cdot CR + (1 - C_d)} \tag{10}$$

$$COP_{Cylce,i} = \frac{Q_{Cond,i}}{W_{System,i}} = \frac{Q_{Cond,design} \cdot Load\%_i}{W_{Comp,i} + W_{Water\ pump,i} + W_{Brine\ pump,i}} \tag{11}$$

in which, as suggested by EN 14511:3:2018 [19], $W_{Water\ pump,\ i}$ and $W_{Brine\ pump,\ i}$ are calculated as follows:

$$W_{Pump,i}\ =\ \frac{W_{Hyd,i}}{\eta_{Pump,i}} = \frac{\dot{V}_i \cdot \Delta P_i}{\frac{0.35744 \cdot \dot{V}_i \cdot \Delta P_i}{1.7 \cdot \dot{V}_i \cdot \Delta P_i + 17 \cdot \left(1 - e^{-0.3 \cdot \dot{V}_i \cdot \Delta P_i}\right)} \cdot \frac{0.49}{0.23}} \tag{12}$$

This formulation ensures realistic performance estimation under variable load conditions, reflecting system behavior during part-load and cycling operation. The values of pressure drop for the secondary fluid pumps are calculated from the condenser and evaporator models.

3. Results and Discussion

The analysis compares the minimum TCO of heat pumps with scroll and turbo compressors at three power levels and for all considered refrigerants. Figure 4 reports the ratio between optimum scroll- and turbo-based TCO, taking as reference (TCO = 100 %) the scroll R32 system. For fluids compatible with both compressor types, direct one-to-one comparison is possible. Fluids are ordered by increasing NBP, and TCO is decomposed into CAPEX and OPEX — blue shades for turbo (dark = CAPEX, light = OPEX) and red/orange for scroll — while column height represents total TCO.

The turbo-compressor driven heat pump feasibility depends mainly on fluid NBP and power level: a higher NBP lowers evaporating pressure, increasing volumetric flow and compressor size, while increasing power produces similar scaling. As the analyzed turbo-compressors employ gas bearings, low-pressure fluids or high-power cases may exceed bearing load capacity; alternative solutions such as active magnetic bearings could extend the feasible range of oil-free designs.

Turbo-compressor solutions proved viable with low-pressure fluids R1234ze(Z) and R1233zd(E) at 5 and 15 kW; with R32 and R290 at 5 and 15 kW or R1234yf at 100 kW; and with R152a, R134, and R1234ze(E) at all power levels. For R1336mzz(E) and R1336mzz(Z), optimization produced atypical geometries and operating parameters that met design-point targets but showed severe off-design limitations, rendering them theoretically feasible (5 kW) yet practically unviable.

Commercial scroll compressors are available only for R32, R290, R152a, R134, and R1234ze(E) at 5 and 15 kW, and for R32 and R1234yf at 100 kW. For the remaining fluids, no suitable models were found in available selection databases, primarily due to low-pressure characteristics and volumetric flows beyond typical scroll compressor limits.

Across all configurations, turbo-driven systems consistently yield lower TCO than the R32 scroll reference. In every one-to-one comparison, the turbo option outperforms the corresponding scroll system, and even the most expensive turbo case remains cheaper than the least expensive scroll configuration. Table 7 summarizes these results. The advantage of the turbo-compressor stems from two combined effects. First, scroll compressors without variable drive have limited part-load adaptability, and are unable to modulate output while maintaining high isentropic efficiency, and therefore perform poorly under partial load. A variable drive allows for a wider power modulation range, at the expense, however, of efficiency. Turbo compressors, operating at variable speed, follow the thermal demand more closely and achieve higher seasonal performance (Figure 5), thus reducing OPEX. The trend holds across all power levels, with SCOP peaking for R152a and nearby fluids. Second, oil-related performance degradation affects scroll systems. Lubrication oil migrates through the circuit (Zehnder [20]), lowering refrigerant performance and causing heat-exchanger fouling. This phenomenon, included in the model, leads to oversized heat exchangers (Figure 6) and increased CAPEX.

Table 7: Refrigerants' percentage optimum TCO of the turbo compressor-based system with respect to the scroll-based one at design power levels 5 kW, 15 kW and 100 kW.

Comparison	5 kW	5 kW	15 kW	15 kW	100 kW	100 kW
	R32	1-to-1	R32	1-to-1	R32	1-to-1
R32		84%		87%		
R290	83%	86%	86%	89%		
R1234yf					99%	92%
R152a	81%	87%	84%	81%	86%	
R134	84%	87%	87%	81%	89%	
R1234ze(E)	90%	89%	94%	84%	96%	
R1336mzz(E)						
R1234ze(Z)	84%		87%			
R1233zd(E)	87%		90%			
R1336mzz(Z)						

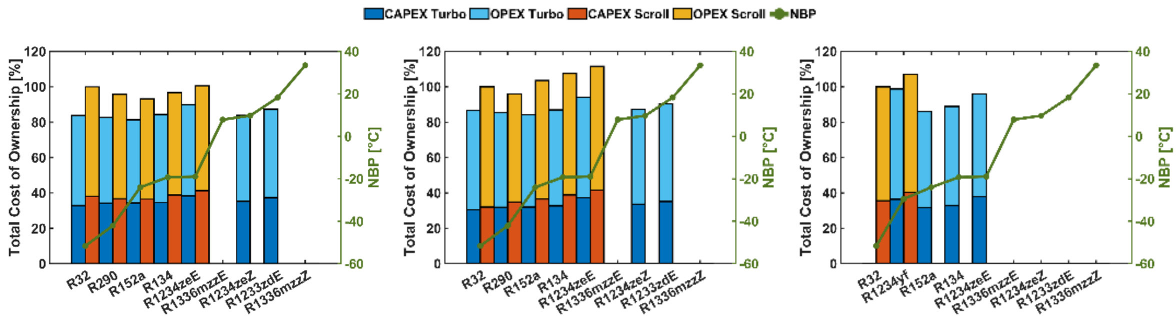

Figure 4. Optimum TCO for turbo and scroll compressor-based systems at different power levels: a) 5 kW, reference cost: $TCO_{R32,scroll}$ = 1,705 [CHF/year], b) 15 kW, reference cost: $TCO_{R32,scroll}$ = 4,490 [CHF/year], c) 100 kW, reference cost: $TCO_{R32,scroll}$ = 27,679 [CHF/year].

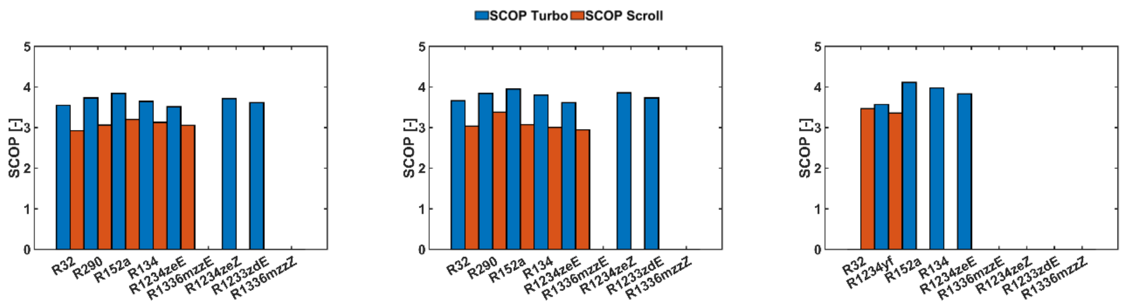

Figure 5. Optimum SCOP for turbo and scroll compressor-based systems at design power levels: (a) 5 [kW], (b) 15 [kW], (c) 100 [kW].

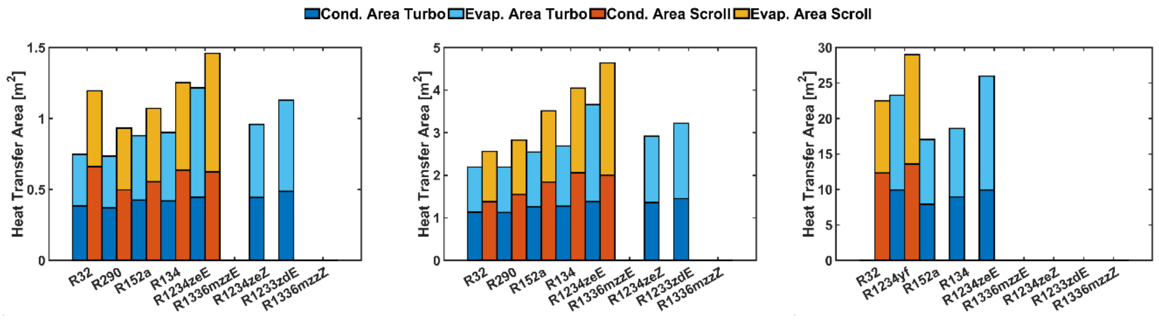

Figure 6. Heat transfer areas for turbo and scroll compressor-based systems at power levels: (a) 5 kW, (b) 15 kW, (c) 100 kW.

4. Conclusions

This analysis highlights a consistent advantage of turbo compressor configurations over scroll-based systems across all power levels, in both CAPEX and OPEX, leading to markedly lower TCO. Scroll systems exhibit several compounded drawbacks — oil-induced fouling, oversized and costlier heat exchangers, limited load modulation, and reduced seasonal efficiency. Oil presence not only degrades thermal performance but also alters optimal design parameters, yielding less efficient configurations.

All turbo-compressor compatible refrigerants outperformed the R32 scroll reference. The best results were obtained with R152a, achieving only 81%, 84%, and 86% of the baseline TCO at 5, 15, and 100 kW, respectively. Even the least favourable turbo case, R1234ze(E), surpassed all scroll systems, reaching 90%, 94%, and 96% of the reference at the same power levels. Turbo compressor driven heat pumps also proved feasible for low-pressure fluids R1234ze(Z) and R1233zd(E) at 5 kW and 15 kW, expanding the viable refrigerant range compared to scroll heat pumps; these reached 84% and 87% of the reference cost at 5 kW and 87% and 90% at 15 kW, respectively.

In direct one-to-one comparisons, turbo systems consistently outperformed scroll counterparts: R152a and R134 achieved 87% and 81% of their scroll-based TCOs at 5 kW and 15 kW, respectively, while at 100 kW, R1234yf reached 92%. Overall, for heat pump capacities between 5 kW and 100 kW, turbo compressors represent a technically and economically superior solution wherever feasible, combining lower cost with higher energy efficiency.

References

[1] IPCC. Summary for policymakers. In: *Climate change 2021: The physical science basis. Contribution of Working Group I to the Sixth Assessment Report of the Intergovernmental Panel on Climate Change.* Masson-Delmotte V, Zhai P, Pirani A, Connors SL, Péan C, Berger S, Caud N, Chen Y, Goldfarb L, Gomis MI, Huang M, Leitzell K, Lonnoy E, Matthews JBR, Maycock TK, Waterfield T, Yelekçi O, Yu R, Zhou B, editors. 2021. In press.

[2] IPCC. Summary for policymakers. In: *Climate change 2022: Mitigation of climate change. Contribution of Working Group III to the Sixth Assessment Report of the Intergovernmental Panel on Climate Change.* Shukla PR, Skea J, Slade R, Al Khourdajie A, van Diemen R, McCollum D, Pathak M, Some S, Vyas P, Fradera R, Belkacemi M, Hasija A, Lisboa G, Luz S, Malley J, editors. Cambridge: Cambridge University Press; 2022. DOI: 10.1017/9781009157926.001.

[3] International Energy Agency (IEA). *Tracking clean energy progress 2023.* Paris: IEA; 2023. Available from: https://www.iea.org/reports/tracking-clean-energy-progress-2023. Licence: CC BY 4.0.

[4] International Energy Agency (IEA). *The future of heat pumps.* Paris: IEA; 2022. Available from: https://www.iea.org/reports/the-future-of-heat-pumps. Licence: CC BY 4.0.

[5] Gaur AS, Fitiwi DZ, Curtis J. *Heat pumps and our low-carbon future: A comprehensive review.* Energy Res Soc Sci 2021; 71: 101764. DOI: 10.1016/j.erss.2020.101764.

[6] Schiffmann J. Small-scale and oil-free turbocompressor for refrigeration applications. In: *Proc. 22nd Int. Compressor Engineering Conf., Purdue University, West Lafayette, IN, USA;* July 14–17; 2014. Paper 2354.

[7] Lemmon EW, Bell IH, Huber ML, McLinden MO. *NIST Standard Reference Database 23: Reference Fluid Thermodynamic and Transport Properties – REFPROP, Version 10.0.* Gaithersburg, MD: National Institute of Standards and Technology, Standard Reference Data Program; 2018.
[8] Melinder A. *Thermophysical properties of aqueous solutions used as secondary working fluids.* TRITA REFR Report No. 07/60. Stockholm: Royal Institute of Technology (KTH), Division of Applied Thermodynamics and Refrigeration; 2007. ISBN 978-91-7178-707-1.
[9] European Committee for Standardization (CEN). *EN 14825:2018 – Air conditioners, liquid chilling packages and heat pumps, with electrically driven compressors, for space heating and cooling — Testing and rating at part load conditions and calculation of seasonal performance.* Brussels: CEN; 2018.
[10] Schiffmann J, Benini E, Fuchs T. *Scale limitations of gas bearing supported turbocompressors for vapor compression cycles.* Int J Refrig 2020; 109: 92–104. DOI: 10.1016/j.ijrefrig.2019.09.019.
[11] Amalfi RL. *Two-phase heat transfer mechanisms within plate heat exchangers: Experiments, modeling and simulations.* PhD Thesis. Lausanne: École Polytechnique Fédérale de Lausanne; 2016. Ch. 8, p. 93.
[12] Sinnott R, Towler G. Chapter 12 – Heat-transfer equipment. In: *Chemical engineering design,* 6th ed. Oxford: Butterworth-Heinemann; 2020. p. 773–927.
[13] Hadka D, Reed P. *Borg MOEA.* Available from: http://borgmoea.org/ (accessed 29 Sep 2025).
[14] Auracher H. *Thermal design and optimization.* Int J Refrig 1996; 19(7): 482. DOI: 10.1016/S0140-7007(97)87632-3.
[15] Wei M, Zhao Y, Li D, Lee H, Ding Y, Sun Y. *Benefits and challenges in deployment of low global warming potential R290 refrigerant for room air conditioning in California.* Sustain Energy Technol Assess 2024; 70: 103937. DOI: 10.1016/j.seta.2024.103937.
[16] Mounier V. *Potential and challenges of ORC driven heat pumps based on gas bearing supported turbomachinery.* PhD Thesis. Lausanne: École Polytechnique Fédérale de Lausanne; 2018. Ch. 4, p. 144.
[17] Olympios AV, Sadafi A, Hashemi A, Schiffmann J. *Data-driven compressor performance maps and cost correlations for small-scale heat-pumping applications.* Energy 2024; 291: 130171. DOI: 10.1016/j.energy.2023.130171.
[18] Henchoz S, Maréchal F, Favrat D. *Performance and profitability perspectives of a CO_2-based district energy network in Geneva's city centre.* Energy 2015; 85: 221–235. DOI: 10.1016/j.energy.2015.03.079.
[19] European Committee for Standardization (CEN). *EN 14511-3:2018 – Air conditioners, liquid chilling packages and heat pumps for space heating and cooling and process chillers, with electrically driven compressors — Part 3: Test methods.* Brussels: CEN; 2018.
[20] Zehnder M. *Efficient air–water heat pumps for high temperature lift residential heating, including oil migration aspects.* PhD Thesis. Lausanne: École Polytechnique Fédérale de Lausanne; 2004.